

# Deep Change Monitoring: A Hyperbolic Representative Learning Framework and a Dataset for Long-term Fine-grained Tree Change Detection

Yante Li  
Univeristy of Oulu  
yante.li@oulu.fi

Hanwen Qi  
Wuhan University  
hanwen.qi@whu.edu.cn

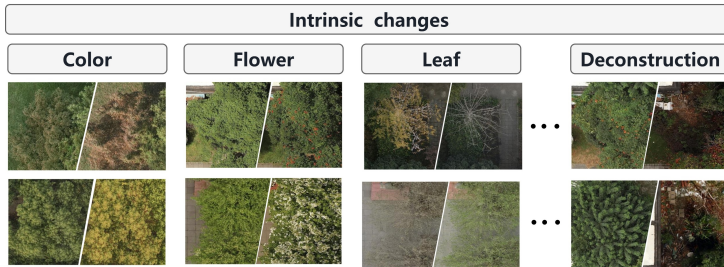
Haoyu Chen  
Univeristy of Oulu  
haoyu.chen@oulu.fi

Xinlian Liang  
Wuhan University  
xinlian.liang@whu.edu.cn

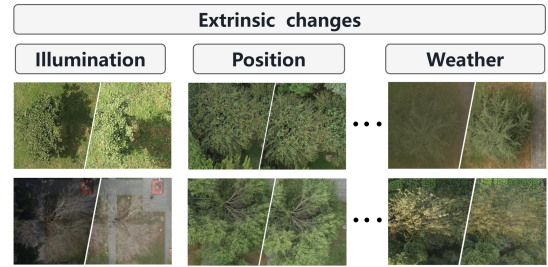
Guoying Zhao  
Univeristy of Oulu  
guoying.zhao@oulu.fi



(a) Tree samples across the entire timeline in the dataset



(b) Examples of tree changes caused by physiological factors



(c) Examples of changes caused by environmental factors

Figure 1. The proposed UAVTC is a dataset for long-term, precise tree monitoring aimed at supporting environmental protection. (a) UAVTC includes a large volume of high-resolution tree images captured by UAVs with cameras over one year. Tree changes encompass intrinsic (b) and extrinsic (c) patterns, which share hierarchical relationships. Traditional linear operators in Euclidean space are ineffective at representing these complex relationships. In contrast, hyperbolic spaces are naturally suited to embedding hierarchies with low distortion [31, 32].

## Abstract

In environmental protection, tree monitoring plays an essential role in maintaining and improving ecosystem health. However, precise monitoring is challenging because existing datasets fail to capture continuous fine-grained changes in trees due to low-resolution images and high acquisition costs. In this paper, we introduce UAVTC, a large-scale, long-term, high-resolution dataset collected using UAVs equipped with cameras, specifically designed to detect individual Tree Changes (TCs). UAVTC includes rich annotations and statistics based on biological knowledge, offering a fine-grained view for tree mon-

itoring. To address environmental influences and effectively model the hierarchical diversity of physiological TCs, we propose a novel Hyperbolic Siamese Network (HSN) for TC detection, enabling compact and hierarchical representations of dynamic tree changes. Extensive experiments show that HSN can effectively capture complex hierarchical changes and provide a robust solution for fine-grained TC detection. In addition, HSN generalizes well to cross-domain face anti-spoofing task, highlighting its broader significance in AI. We believe our work, combining ecological insights and interdisciplinary expertise, will benefit the community by offering a new benchmark and innovative AI technologies. Source code

is available on <https://github.com/liyantett/Tree-Changes-Detection-with-Siamese-Hyperbolic-network>.

## 1. Introduction

Forests, essential for climate stability and ecological health, act as crucial biological reserves [12, 47]. Effective forestry and management hinge on diligent tree monitoring, which includes growth measurement, health assessment, and environmental impact analysis, and so on [48]. One of the key aspects of tree monitoring is Tree Change Detection (TCD). TCD identifies alterations in tree conditions, essential for tree management and overall forest ecosystem health.

*This research aims to accomplish long-term fine-grained TCD with deep learning methods.* Fine-grained TCD is critical yet challenging, especially when collecting long-term, high-resolution data in forests under diverse environmental conditions. Leveraging Unmanned Aerial Vehicles (UAVs) with cameras for forest imagery collection has become popular for its convenience and accessibility, offering an efficient alternative to traditional methods like LiDAR for large-scale data collection, essential for monitoring trees and ecological sustainability [40]. Thus, to boost data-driven learning methods for the research field, this paper introduces a UAV-camera-based dataset tailored for detecting individual Tree Changes (UAVTC), enabling precise tree monitoring, as shown in Figure 1 (a). *To our knowledge, UAVTC is the first dataset to provide detailed insights into precise TCs over time, supporting sustainable forest management and ecological research.*

*The primary challenge in TCD lies in identifying extrinsic changes driven by the environments and intrinsic changes referring to physiological processes.* As shown in Figure 1 (c), environmental factors such as fog and direct sunlight can obscure views and cast shadows, leading to non-tree-related changes. These extrinsic changes can mislead and result in incorrect TCD. Apart from extrinsic changes, physiological TCs are inherently hierarchical, involving both growth and decay processes. These changes can be classified into four main categories: changes in color, leaf transformations, flowering and fruiting cycles, and damage caused by humans, as shown in Figure 1 (b). These diverse attributes of trees give rise to complex hierarchical relationships between TCs caused by environmental and physiological factors, which are not effectively captured by Euclidean geometry. Instead, hyperbolic geometry provides a solution by faithfully representing tree-like structures [22], making it ideal for modeling and understanding physiological TCs.

To address the above issues, we propose a Hyperbolic Siamese Network (HSN) designed to effectively model hierarchical changes and mitigate the impact of environmental factors, thereby enabling efficient identification of physiological TCs. HSN achieves this by (1) **Modeling Hierarchical Structure**: HSN encodes hierarchical relationships

present in changes driven by environmental factors and intrinsic physiological changes at distinct levels, clarifying the pathways and impacts of each change; (2) **Optimizing Data Embedding and Representation**: Hyperbolic space allows for an efficient low-dimensional representation of high-dimensional hierarchical relationships, enabling both environmental and physiological changes to be effectively embedded and analyzed for structural and influential similarities or differences; (3) **Modeling Spatiotemporal Dynamics**: To model changes between tree images taken at different time points, we designed a network that integrates a Siamese structure within hyperbolic space. The Siamese network structure within hyperbolic space enhances analysis of dynamic changes across time and space, enabling clearer insights into trees' responses to complex interactions between environmental conditions and physiological factors.

To the best of our knowledge, this is the first hyperbolic network designed specifically for change detection. *Thus, we also provide extra experiments on cross-domain face anti-spoofing (CD-FAS), showing that HSN excels at managing complex real-world changes involving extrinsic and intrinsic patterns.*

The main contributions are as follows:

- We collect a large-scale UAVTC dataset for long-term fine-grained TCD. To the our best knowledge, the UAVTC is the first TCD dataset that is collected from UAV devices, which contains rich annotations and statistics, covering multiple aspects of tree growth and health, enabling fine-grained tree monitoring over time.
- We propose a novel Hyperbolic Siamese Network to model tree changes in hyperbolic space, overcoming misleading caused by extrinsic factors and effectively capturing the intrinsic tree changes.
- Extensive experiments demonstrate that HSN is highly effective for fine-grained tree monitoring and can be generalized to CD-FAS task, highlighting its versatility and robustness.

## 2. Related work

### 2.1. Tree monitoring dataset comparison

Forest monitoring is crucial for effective tree management and policy development. Remote sensing provides continuous, all-weather, multi-spectral observations to detect forest changes with precision. While spaceborne platforms offer broad land cover data, their limited resolution is insufficient for detailed forest analysis [15, 35]. In contrast, UAVs provide more frequent and closer-range observations [2, 34].

UAVs equipped with LiDAR technology are capable of generating accurate 3D models of trees, offering key data such as tree height, area, and volume growth through spatial coordinates and surface reflectivity measurements [41, 48]. However, LiDAR lacks the capability to capture color or

Table 1. UAV-camera-based tree datasets. Our dataset offers large-scale, high-resolution tree images accompanied by fine-grained TC annotations. In terms of resolution ( $cm/pixel$ ), the lower value represents the better performance.

Dataset	Task	Resolution ↓ ( $cm/pixel$ )	Test site size ( $m$ )	Duration (Month)	Flight days	Image / Image pairs	Publicly available
[28]	Leaf coverage	7	1000×500	12	34	2,422	×
[3]	Treefall detection	5	1000×500	60	60	60	✓
[24]	Flower recognition	5	1000×500	24	21	34,713	×
UAVTC (Ours)	TCD (color, blossom, leaf, branch)	0.5	110×140	12	85	245,616	✓

✓ indicates the datasets is publicly available; × signifies it’s not.

↓ represents the lower value with the better performance.

intricate texture details, thus limiting its ability to reflect TCs [30].

Instead, UAVs equipped with RGB cameras excel in capturing long-term tree changes that include color and texture details. Park et al. [28] conducted leaf phenology research in a 50 ha tropical forest using a UAV equipped with an RGB camera. Similarly, Lee et al. [24] employed this technology to identify flowering patterns of various tree species over five years with 34,713 images. Additionally, a five-year dataset of monthly drone-captured RGB images was analyzed to track treefall and branchfall in Panama [3], offering deep insights into forest dynamics. However, the above studies focus on singular aspect of tree states, such as blossoming or branch falling, without a comprehensive view of the TCs over time. Comparing trees over time is vital for understanding growth, health, and environmental responses, enabling early disease detection and guiding forest management, ecological research, and conservation efforts, ultimately crucial for biodiversity and ecosystem sustainability.

To bridge this gap, our paper presents the UAVTC dataset, facilitating the observation of fine-grained TCs across multiple aspects and allowing for the comparison of individual trees over time. The UAVTC includes color changes, branch modifications, blossom, and more, averaging nearly once a week with a resolution of 0.5 cm/pixel. It presents a unique resource for achieving detailed tree monitoring with 245,616 tree image pairs, covering a wider spectrum of TCs than previously available datasets. The specific comparison of UAVTC with other existing datasets is illustrated in Table 1.

## 2.2. Hyperbolic geometry

Hyperbolic geometry, characterized by a constant negative Gaussian curvature, has proven to be beneficial for hierarchical relationships between images, and representing tree-like structures, taxonomies, and graphs [1, 22, 26]. There are five isometric models of hyperbolic geometry [6]: the Lorentz (hyperboloid) model, Klein model, Hemisphere model, Poincaré ball, and Poincaré ball half-space model. Among these models, the Poincaré ball model has been dominated in the hyperbolic deep neural networks due to its differentiable distance function and the simplicity of its

constraints on representations.

Maximilian et al. [26] first introduced the Poincaré model for embedding learning, taking into account latent hierarchical structures. Their research demonstrated that Poincaré embeddings exhibit superior performance compared to Euclidean embeddings, especially in datasets characterized by latent hierarchies. Recently, hyperbolic embeddings have been very successful in the natural language processing field [27, 31, 32]. However, the above works utilized Riemannian optimization algorithms to embed individual words into hyperbolic space due to the discrete nature of data in natural language processing. Extending this method to visual data proves challenging, as image representations are commonly generated with convolutional neural networks [22].

Khrulkov et al. [22] investigated the hybrid architecture with the convolutional neural networks operating in Euclidean space and only the final layers operating in hyperbolic space. This research verifies the effectiveness of capturing semantic and hierarchical information in images by the hyperbolic network. Then, Hyperbolic Networks (HNs) have been successfully developed for various computer vision tasks including image segmentation [4, 7], action recognition [29], face recognition [19, 42], and metric learning [13, 16, 17]. In summary, hyperbolic geometry proves instrumental in diverse applications, and its incorporation into deep learning frameworks enhances the representation of hierarchical relationships and semantic similarities in various types of data, including images, text, and graphs. Considering the complex hierarchical relationships in intrinsic TCs and noises caused by environments, this paper presents utilizing hyperbolic space to effectively analyze and understand TCs. The HSN offers a new perspective and enhanced capabilities for capturing the complex and hierarchical changes.

## 3. UAV-camera-based TC dataset collection

### 3.1. Test site and equipment

To study fine-grained TCs, this paper presents a comprehensive tree dataset by UAV equipped with an RGB camera. The experiment was carried out in a  $110m \times 140m$  plot in a mixed urban forest. The species mainly include

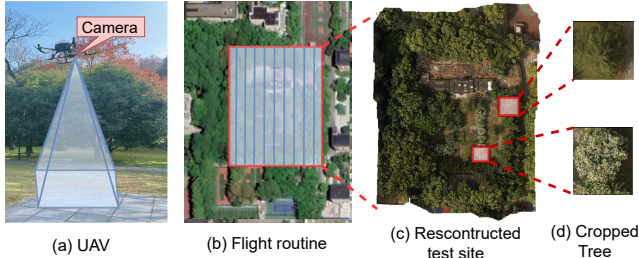


Figure 2. The illustration of the data collection process. (a) the UAV equipped with a camera (DJI Zenmuse P1), (b) the flight routine outlining the test site, (c) the reconstructed test site after the UAV has captured the necessary imagery, and (d) the final cropped tree images.

Camphora officinarum, Cedrus, firethorn, and Malus mandshurica. Some species are evergreen and non-flowering plants, such as Camphora officinarum and Cedrus, while other species may blossom and even yield fruit.

The platform utilized in this paper is DJI M300 RTK (DJI Innovations), and the camera is DJI Zenmuse P1 (lens FOV 63.5 degrees, focus length 35mm, Max image size  $8192 \times 5460$  pixels), As shown in Figure 2 (a). Both the front and side overlapping in between photos were set to 80% and the flight altitude was 50m above the ground, and the flight speed was 3m/s. The shutter was set to 1/400 on bright days, when the sunlight was not sufficient, the shutter could be set to 1/200. In addition, ISO was set to 100 and F was 2.8. During the data collection process, the UAV followed a predefined flight routine, as illustrated in Figure 2 (b). Typically, each flight mission resulted in the capture of approximately 220 pictures of the test site. Moreover, Digital Orthophoto Model (DOM) was produced by DJI Terra (Figure 2 (c)), and geographic registration root mean square error was within 4cm, RMS of reprojection error was within 1px. For more details about the dataset collection, please refer to the supplementary material.

### 3.2. Preprocessing and annotation

The goal is to detect changes in individual trees, necessitating the acquisition of their respective regions of interest (ROIs). Each tree was individually outlined with a rectangle in ENVI software, based on GPS coordinates from the tree data gathered on 07/11/2022. Since each DOM was projected to the same coordinate system, it was straightforward to crop according to the ROI. The ROI was determined using the four corners of a rectangle, slightly larger than the tree crown to ensure full coverage, accounting for potential crown growth. Figure 2 (c) illustrates two representative cropping of trees, the red transparent rectangles are the ROIs, and the two individual trees are shown in Figure 2 (d).

To evaluate the change, the annotation process is divided into two steps. Firstly, two forest experts independently annotated the tree’s states. In cases of disagreement, the final

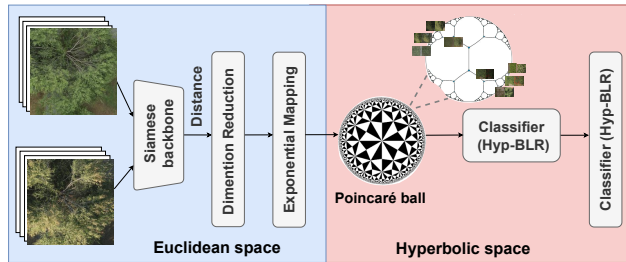


Figure 3. Framework of Hyperbolic Siamese Network. First, features extracted from the backbone Siamese network undergo a comparison process to compute change. Subsequently, a fully connected (FC) layer reduces the dimension of the change feature. The model utilizes exponential mapping to transform embeddings from the Euclidean space to hyperbolic space. A Hyp-BLR is followed for the classification. Finally, a Hyp-BCE loss function is employed to train modes for TCD.

state was determined through a consensus reached by these experts after discussion. Specifically, a total of six states are considered including green leaf, yellow leaf, branch, fallen leaves or sprout, blossom, and destroy. The inconsistent states indicate the presence of tree changes, otherwise is no change. For more details about the data annotation, please refer to the supplementary material.

### 3.3. Data statistics

The tree images were collected from 07/10/2022 to 03/11/2023. Data collection is usually performed between 2 p.m. and 4 p.m., as often as possible once every two days, but sometimes once every three or four days due to weather conditions, such as rain or strong winds, and on average two or three times a week. A total of 85 time points capturing the changes in trees over one year were collected. 68 trees were selected and cropped for analysis. The trees are in diversity, from evergreen to deciduous, flowering, and fruit-bearing trees. Despite the limited number of trees, which may influence the generalizability of the model, the dataset’s diversity sufficiently supports robust model training for individual tree change detection. To thoroughly investigate tree changes, we perform a pairwise comparative analysis of tree images at all time points for each tree. In total, we have 245,616 pair tree images. 72% belongs to change and 28% belongs to no change. The average pixels for each tree ROI is around  $2000 \times 2000$  pixels.

## 4. Methodology

In this section, we introduce the technical details of the HSN for TCD. The schematic overview of the proposed method is depicted in Figure 3. First, we introduce the operations in hyperbolic spaces in Section 4.1. Hyperbolic feature clipping for model optimization is described in Section 4.1. Then we describe the hyperbolic Siamese architecture.

Hyperbolic cross-entropy loss is introduced in Section 4.3. Finally, we compute the  $\delta$ -hyperbolicity on the embeddings of TCs, theoretically verifying the presence of hierarchical structures within the TCs.

#### 4.1. Hyperbolic operations

As highlighted in the Introduction section, TCD is significantly influenced by environment conditions and characterized by hierarchical structures. Prior studies have shown that hyperbolic geometry effectively captures data hierarchies, enhancing robustness and accuracy by mitigating the impacts of extrinsic factors like weather variants[22]. Therefore, hyperbolic geometry is utilized in this paper. Specifically, our research utilizes the Poincaré ball model [26], as the Poincaré ball possesses a differentiable distance function and is characterized by a relatively simple constraint on its representations. These strengths make it suitable for TCD research.

Formally, the  $n$ -dimensional Poincaré ball  $(\mathbb{H}_c^n, g^{\mathbb{H}})$  is defined by the manifold  $\mathbb{H}_c^n$  as

$$\mathbb{H}_c^n = \left\{ X \in \mathbb{R}^n : c \|x\|^2 < 1, c \geq 0 \right\}, \quad (1)$$

and the Riemannian metric  $g^{\mathbb{H}}$  is

$$g_x^{\mathbb{H}} = \lambda_x^{c^2} g^{\mathbb{E}}, \quad (2)$$

where  $g^{\mathbb{E}}$  is the Euclidean metric tensor and  $\lambda_x^c$  is the conformal factor defined as  $\lambda_x^c = \frac{2}{1-c\|x\|^2}$ .  $g^{\mathbb{H}}$  is associated with tangent space  $T_x$ . Note,  $c^{-\frac{1}{2}}$  is the radius of Poincaré ball.  $c$  controls the the curvature of the Poincaré ball. As  $c$  approaches 0, operations revert to Euclidean geometry.

Hyperbolic spaces differ from traditional vector spaces, making standard operations like addition and multiplication unusable. Möbius gyrovector spaces offer a solution to generalize these operations. Key operations for hyperbolic networks are described below.

**Möbius addition.** Möbius gyrovector spaces offer a means to define operations like addition and multiplication. These operations are fundamental in hyperbolic networks [22]. For a pair  $x, y \in \mathbb{H}_c^n$ , their addition is defined as

$$x \oplus_c y = \frac{(1 + 2c\langle x, y \rangle + c\|y\|^2)x + (1 - c\|x\|^2)y}{1 + 2c\langle x, y \rangle + c^2\|x\|^2\|y\|^2}. \quad (3)$$

**Distance.** In hyperbolic geometry, the distance between two points,  $x, y \in \mathbb{H}_c^n$ , is defined as

$$d_{\text{hpy}}(x, y) = \frac{2}{\sqrt{c}} \operatorname{arctanh}(\sqrt{c}\| -x \oplus_c y \|). \quad (4)$$

When  $c$  approaches 0, the hyperbolic distance function converges to the Euclidean distance. This convergence is expressed as  $\lim_{c \rightarrow 0} d_{\text{hpy}}(x, y) = 2\|x - y\|$ .

**Exponential map.** To conduct operations in hyperbolic space, it is necessary to establish a bijective mapping between Euclidean vectors and hyperbolic vectors in the Poincaré ball model. The pivotal tool for this purpose is the exponential map. The map establishes a one-to-one correspondence between points from Euclidean space to points in hyperbolic space. The exponential map is formulated as:

$$\exp_x^c(v) = x \oplus_c \left( \tanh\left(\sqrt{c} \frac{\lambda_x^c \|v\|}{2}\right) \frac{v}{\sqrt{c}\|v\|} \right). \quad (5)$$

**Hyperbolic binary logistic regression (Hpy-BLR).** In the context of the TCD task, two classes are established: when  $k = 0$ , it indicates the absence of change, and when  $k = 1$ , it denotes the presence of change and  $p_k \in \mathbb{H}_c^n$ ,  $t_k \in T_{p_k} \mathbb{H}_c^n \setminus \{0\}$ . The formulation of binary logistic regression within the Poincaré ball is expressed as follows:

$$p(y = k | x) \propto \exp\left(\frac{\lambda_{p_k}^c \|t_k\|}{\sqrt{c}} \operatorname{arcsinh}\left(\frac{2\sqrt{c}\langle -p_k \oplus_c x, t_k \rangle}{(1 - c\| -p_k \oplus_c x \|^2)\|t_k\|}\right)\right). \quad (6)$$

**Feature clipping.** Previous research [17, 18] provides empirical evidence indicating that HNs often experience the issue of vanishing gradients. This occurs because HNs tend to drive embeddings towards the boundary of the Poincaré ball, resulting in the gradients of Euclidean parameters becoming extremely small. To mitigate potential numerical errors, a fixed threshold is applied to the norm (magnitude) of the vectors to prevent them from reaching extreme values [17], following the equation below:

$$C(x^E; r) = \min\left\{1, \frac{r}{\|x^E\|}\right\} \cdot x^E \quad (7)$$

where  $x^E$  lies in the Euclidean space and  $x_C^E$  represents its clipped counterpart. The hyperparameter  $r$  denotes a novel effective radius within the Poincaré ball. This feature clipping method imposes a hard constraint on the maximum norm of the hyperbolic embedding which avoids the inverse of the Riemannian metric tensor approaching zero [17].

#### 4.2. Hyperbolic Siamese framework

What is the desired representation for TC? We argue that such representation should effectively present the precise physiological change in trees and maintain robustness to changes caused by extrinsic factors. To achieve the above goals, we train an HSN (shown in Figure 3) consisting of Siamese framework and hyperbolic geometry. The key objectives of this approach are 1) accurately evaluating TCs and 2) learning robust features avoiding misleading influences from extrinsic factors.

For a classical Siamese network [10, 23], the input is a pair of images, represented as  $I_1$  and  $I_2$ . The Siamese

network learns to project inputs into a space where the distance between similar inputs is minimized, and the distance between dissimilar inputs is maximized, facilitating tasks such as similarity comparison or verification [8]. Specifically,  $f(I; W)$  is the output of the Siamese network, where  $W$  represents the parameters of the network. A common choice the measure the feature distance is the Euclidean distance:

$$D(I_1, I_2) = \|f(I_1; W) - f(I_2; W)\|, \quad (8)$$

However, as discussed in the introduction section, TCs include a hierarchical structure that can not be effectively estimated by the flat Euclidean space. Instead, hyperbolic space characterized by negative curvature has been found to be well-suited for representing hierarchical relationships. The hyperbolic space is leveraged to represent complex TCs with hierarchy. Firstly, a fully connected (FC) layer is employed to reduce the dimension of the change feature. Then the Euclidean distance embedding is transformed to hyperbolic distance by exponential mapping with Equation 5. A Hyp-BLR layer is followed for classification. Finally, the Hyp-BCE loss function (Equation (9)) is employed to identify and assess the changes in trees.

### 4.3. Hyperbolic binary cross entropy loss

The Hyperbolic Binary Cross Entropy (Hpy-BCE) loss is calculated using the predicted probability  $\hat{p}_i$  obtained from Equ. 6. The loss is defined as:

$$L_a = p_i \log(\hat{p}_i) + (1 - p_i) \log(1 - \hat{p}_i), \quad (9)$$

where  $p_i$  is the ground truth for changes in a tree, with 1 denoting a change in the tree and 0 denoting no change.  $\hat{p}_i$  is the predicted probability of TC.

### 4.4. $\delta$ -Hyperbolicity

In this section, we validate the presence of hierarchical structures in TC data through  $\delta$ -hyperbolicity [22]. This metric serves to quantify the similarity in data structure between Euclidean and hyperbolic space. The  $\delta$ -hyperbolicity values range from 0 to 1, where a calculated value closer to 0 indicates a high degree of hyperbolicity in the data, signifying a strong hierarchy. Conversely, a computed  $\delta$ -hyperbolicity closer to 1 suggests the absence of hierarchy in the dataset.

This hyperbolicity evaluation is made through Gromov product [14]:

$$(y, z)_x = \frac{1}{2}(d(x, y) + d(x, z) - d(y, z)) \quad (10)$$

where  $x, y, z \in \chi$  and  $\chi$  is the arbitrary (metric) space endowed with the distance function  $d$ . Given a set of points, we compute the pairwise Gromov products and represent them in the form of a matrix  $A$ . Subsequently, the value of  $\delta$  is identified as the maximum element in the matrix obtained from the min-max matrix product operation, denoted

as  $(A \oplus A) - A$ . In this context, the symbol  $\oplus$  represents the min-max matrix product, which is formally defined as  $(A \oplus B)_{ij} = \max_k \min \{A_{ik}, B_{kj}\}$  [14].

We evaluate  $\delta$  for tree image embeddings extracted by Siamese networks with ResNet18 [20], ResNet34, ResNet101, and VGG16 [36]. Table 2 demonstrates the obtained relative  $\delta$  values. Table 2 shows that all networks exhibit low  $\delta$  (closer to 0 than 1), indicating high hyperbolicity in the tree change dataset. This observation suggests that TCD tasks can benefit from hyperbolic representations of images and the experiments in Section 5 verify the effectiveness of hyperbolic representations.

Table 2.  $\delta$ -Hyperbolicity. Low  $\delta$  (closer to 0 than 1) indicates a high degree of hyperbolicity in the embeddings.

Network	ResNet18	ResNet34	ResNet101	VGG16
$\delta$	0.172	0.144	0.114	0.212

## 5. Experiments

In this section, we first introduce the protocols, evaluation metrics, and implementation details in this paper. Then, we evaluate the impacts of hyperparameters. Finally, We show the baselines on our constructed tree change dataset and the improvements with hyperbolic spaces on both TC and CD-FAS tasks.

### 5.1. Protocols and evaluation matrix

TCD task is to detect whether there are changes between trees at different time points to monitor climate change and protect the environment automatically. In the experiment, around two-thirds of the trees (44 trees) were used as the training data, while one-third (24 trees) were reserved for testing. Since 85 flight days were collected, there are 158,928 image pairs for training and 86,688 image pairs for testing.

Both accuracy and F1-score are utilized to evaluate the performance of TCD. In binary classification tasks, especially with imbalanced samples, it is better to incorporate F1-score with accuracy to interpret the algorithm performance.

### 5.2. Implementation details

For training Euclidean Siamese networks (ESNs), we employ SGD with momentum, while HSNs are trained with the AdamW optimizer [25]. All the networks are fine-tuned on ImageNet [11] and trained for 30 epochs. We use an initial learning rate of  $1 \times 10^{-6}$  for convolutional layers, 0.001 for FC layers, and 0.1 for hyperbolic layers. The learning rate decays by 10 every 10 epochs. The batch size is 128. In the training stage, the images are resized to  $256 \times 256$  ( $310 \times 310$  for HS-InceptionV3) and randomly cropped to  $224 \times 224$  ( $299 \times 299$  for HS-InceptionV3). In the testing stage, images are captured with a resolution of  $224 \times 224$

Table 3. The impacts of the parameter  $c$  used in HSNs.

$c$	ACCURACY					F1				
	0.1	0.3	0.5	0.7	1.0	0.1	0.3	0.5	0.7	1.0
HS-ResNet18	80.71	<b>80.80</b>	79.69	79.74	80.27	<b>0.6156</b>	0.6053	0.5907	0.5754	0.6057
HS-ResNet34	81.43	<b>81.86</b>	80.08	80.02	81.00	<b>0.6479</b>	0.6449	0.5790	0.5813	0.6300
HS-ResNet101	86.50	85.60	86.18	86.15	<b>86.83</b>	0.7204	0.6877	0.7137	0.7127	<b>0.7372</b>
HS-VGG16	74.02	<b>77.18</b>	74.60	74.55	72.29	0.5805	<b>0.6101</b>	0.5841	0.5756	0.5455
HS-InceptionV3	76.55	77.08	<b>77.23</b>	76.50	77.14	0.6552	<b>0.6556</b>	0.6481	0.6447	0.6467
HS-MobileNet	77.05	76.73	76.79	77.56	<b>77.74</b>	0.4822	0.4979	<b>0.5048</b>	0.4858	0.4953

Table 4. Ablation study of each module.

Method	ACCURACY	F1
Siamese network	82.09	0.5947
Siamese network+HL	85.35	0.7164
Siamese network+HL+FCLP	<b>86.83</b>	<b>0.7372</b>

using a center crop ( $299 \times 299$  for HS-InceptionV3). The clipping radius (defined in Section 4.4)  $r = 2.3$ , following [13]. The random seed is set to 42.

### 5.3. Ablation study

**Manifold curvature.** As illustrated in Sections 4.1, the value of  $c$  represents the manifold curvature of a Poincaré Ball model. To comprehensively analyze the impacts of the parameter  $c$ , experiments were conducted on UAVTC dataset with  $c = \{0.1, 0.3, 0.5, 0.7, 1.0\}$ . The feature dimensions were fixed with eight. Table 3 shows the HSN performances depending on the curvature value  $c$ . From Table 3, we find that the methods are relatively robust in the range (0.1, 1.0). In general, the deeper networks could achieve better performance with higher  $c$ . Specifically, HS-ResNet101 performs best with  $c = 1.0$ , while HS-ResNet18 and ResNet34 achieve optimal F1-scores with  $c = 0.1$ . The results suggest that shallow networks tend to learn embeddings in a manifold with flatter curvature, whereas deep networks display a trend towards learning in manifolds with more pronounced curvature.

**Ball dimension** Due to the exponential growth of hyperbolic space volume with radius, the necessary embedding dimension for representing features can be notably lower than that required in Euclidean space. We investigate the performance of HSNs regarding different Poincaré ball embedding dimensions, as shown in Figure 4. From Figure 4, it can be seen that there is an improvement trend in performance as the dimension of the image embedding increases from 2 to 32. However, with a further increase, the performance begins to decline. This is likely because while initial gains from higher dimensions improve data complexity capture, excessive dimensions eventually cause overfitting, diminishing the model’s effectiveness.

**Hyperbolic module.** In this section, we conduct an ablation study to evaluate the contribution of each component in HSNs. As shown in Table 4, the integration of Hierarchical Learning (HL) into the baseline model leads to a significant improvement in its performance by 20% in terms of

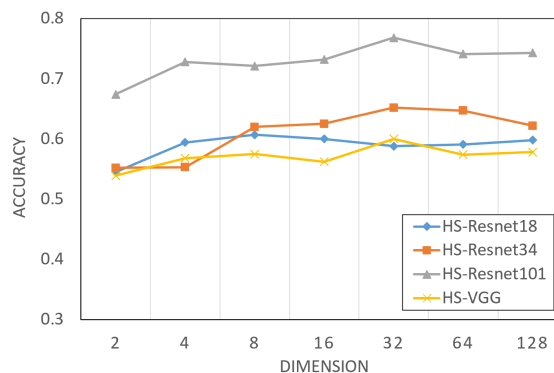


Figure 4. The impacts of the embedding dimensions used in HSNs.

F1-score. Moreover, the incorporation of Feature Clipping (FCLP) boosts the F1-score, from 0.7164 to 0.7372. These improvements verify the effectiveness HL and FCLP.

### 5.4. Benchmark evaluations

In this section, we provide the baselines of TCD, and verify the effectiveness of HSN. Due to limited research on fine-grained change detection, the comparison methods are also limited. The state-of-the-art (SoTA) method cost-effective tree-blossom recognition [24], ResNet101, VGG16, InceptionV3 [39], and MobileNet [37] are utilized. The results are shown in Table 6. It can be seen the HSN outperforms all other listed methods. The HSN achieves the highest accuracy of 86.83% and an F1-score of 0.7372, significantly surpassing other approaches such as ResNet101, InceptionV3, MobileNet, and Tree-blossom recognition, by 24.0%, 29.9%, 60.5%, and 35.2% in terms of F1-score, respectively. These results highlight the superiority of the HSN in terms of precision and reliability in TCD. We can draw a conclusion that there is hyperbolicity in TCD and the HSN can better represent TCs with hyperbolicity. For more comparison results, please refer to the supplementary material.

Figure 5 shows the visualizations of training and testing image embeddings utilizing t-SNE for dimensionality reduction and visualization [43]. The image embeddings were extracted by the Siamese network in Euclidean space and hyperbolic space with Resnet101 as the backbone. From Figure 5, it is evident that the HSN exhibits tighter clustering of same-category data points compared to the Euclidean-based networks, indicating that the network

Table 5. Evaluation of CD-FAS among CASIA (C), Idiap Replay (I), MSU-MFSD (M), and Oulu-NPU (O) databases.

Method (%)	OCI → M (HTER↓/AUC↑)	OMI → C (HTER↓/AUC↑)	OCM → I (HTER↓/AUC↑)	ICM → O (HTER↓/AUC↑)
SSDG-R [21]	14.65 / 91.93	28.76 / 80.91	22.84 / 78.67	15.83 / 92.13
SSAN-R [45]	21.79 / 84.06	26.44 / 78.84	35.39 / 70.13	25.72 / 79.37
PatchNet [44]	25.92 / 83.43	36.26 / 71.38	29.75 / 80.53	23.49 / 84.62
SA-FAS [38]	13.17 / 94.17	24.48 / 85.55	19.79 / 87.95	14.23 / 93.29
Ours	<b>11.98 / 94.33</b>	<b>17.46 / 90.89</b>	<b>18.75 / 89.54</b>	<b>13.45 / 94.34</b>

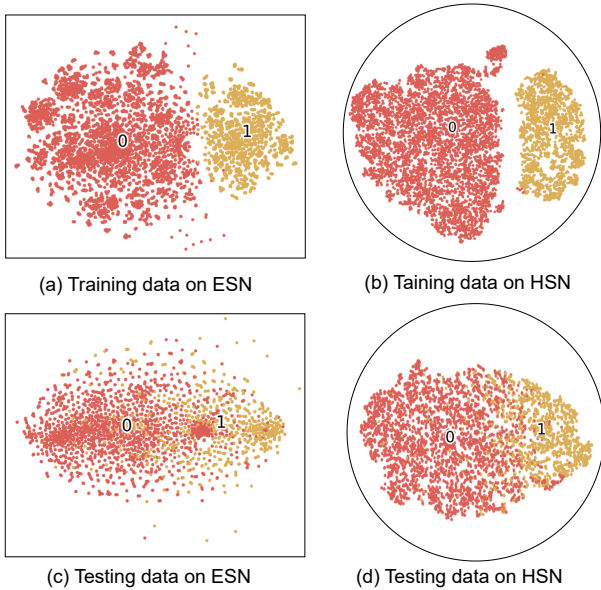


Figure 5. The visualizations on Euclidean and hyperbolic spaces with t-sne [43], respectively. ESN and HSN represent Siamese networks on Euclidean space and hyperbolic space, respectively, on UAVTC.

Method	ACCURACY	F1
ResNet101 [20]	82.09	0.5947
VGG16 [36]	79.21	0.5716
InceptionV3 [39]	78.48	0.5673
MobileNet [37]	76.83	0.4592
Tree-blossom recognition [24]	78.82	0.5413
HSN (Ours)	<b>86.83</b>	<b>0.7372</b>

is learning more uniform and distinctive features in hyperbolic space. Furthermore, Figure 6 displays class activation maps of TC [33]. The HSN appears to effectively concentrate on the tree regions, successfully avoiding misinterpretations caused by shadow and background. More visualization examples are shown in the supplementary material.

### 5.5. Complexity of Hyperbolic Operations

Hyperbolic operations are more computationally intensive compared to Euclidean ones. To mitigate this, we integrated hyperbolic operations with CNN, employing them primarily in the final layer to maintain efficiency. On average, one iteration takes 0.4358 seconds for the Euclidean siamese network and 0.4437 seconds for HSN. It indicates while hyperbolic operations may incur some overhead, our approach balances computational complexity with perfor-

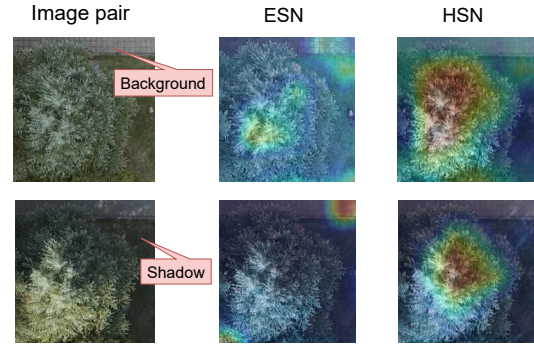


Figure 6. The visualizations of tree change with Gradcam.

mance gains.

### 5.6. Evaluation on CD-FAS

To further prove the effectiveness and impacts of HSN, we evaluate its performance on CD-FAS tasks. CD-FAS differentiates genuine human faces from counterfeit representations in biometric authentication systems across different domains. CD-FAS involves identifying complex variations and changes among extrinsic factors, such as face coverings and lighting conditions, as well as intrinsic factors such as skin texture and material properties. Four popular benchmark datasets are utilized: Oulu-NPU (O) [5], CASIA (C) [49], Idiap Replay Attack (I) [9], and MSU-MFSD (M) [46], highlighting its significance in AI. Leave-one-out test protocol to evaluate their cross-domain generalization.

For fair comparisons with SoTA methods [21, 38, 44, 45], we use the same ResNet-18 backbone. We adapt the learning strategy and evaluation protocol of SA-FAS, employing metrics such as Half Total Error Rate (HTER) and Area Under the Curve (AUC). More implementation details are provided in the Supplementary materials.

From Table 5, we can see that our method based on HSN outperforms SoTA methods in CD-FAS [21, 38, 44, 45] in terms of HTER and AUC. The results further validate the superiority of HSN on change identification, demonstrating its broad impact on the AI community. Additional results and analysis are included in Supplementary materials.

## 6. Conclusion

This paper presents a UAV-camera Tree change (UAVTC) dataset for fine-grained monitoring trees over time and a novel Hyperbolic Siamese Network (HSN) for accurately detecting tree changes. The HSN is able to effectively dis-



tinguish physiological tree changes from extrinsic changes driven by environment variants. Our extensive experiments confirm the hierarchical nature of tree change and the superior performance of the HSN illustrates a significant advancement in the field of precision forestry. Our multidisciplinary research on tree monitoring sets new benchmarks and introduces cutting-edge AI technologies, enhancing ecosystem and biological understanding. Furthermore, the HSN generalizes well to change-identification applications, such as cross-domain face anti-spoofing tasks, underscoring its significance in AI.

In the future, we aim to enhance the dataset to encompass tree segmentation and classification tasks. This expansion could significantly benefit biodiversity research and lead to more precise and all-encompassing approaches in forest management.

## References

- [1] Rami Aly, Shantanu Acharya, Alexander Ossa, Arne Köhn, Chris Biemann, and Alexander Panchenko. Every child should have parents: a taxonomy refinement algorithm based on hyperbolic term embeddings. *arXiv preprint arXiv:1906.02002*, 2019. 3
- [2] Vince Ambrosia, Mike Hutt, and Kamlesh Lulla. Unmanned airborne systems (uas) for remote sensing applications, 2011. 2
- [3] Raquel Fernandes Araujo, Samuel Grubinger, Carlos Henrique Souza Celes, Robinson I Negrón-Juárez, Milton Garcia, Jonathan P Dandois, and Helene C Muller-Landau. Strong temporal variation in treefall and branchfall rates in a tropical forest is related to extreme rainfall: results from 5 years of monthly drone data for a 50 ha plot. *Biogeosciences*, 18(24):6517–6531, 2021. 3
- [4] Mina Ghadimi Atigh, Julian Schoep, Erman Acar, Nanne Van Noord, and Pascal Mettes. Hyperbolic image segmentation. In *Proceedings of the IEEE/CVF conference on computer vision and pattern recognition*, pages 4453–4462, 2022. 3
- [5] Zinelabinde Boulkenafet, Jukka Komulainen, Lei Li, Xiaoyi Feng, and Abdenour Hadid. Oulu-npu: A mobile face presentation attack database with real-world variations. In *2017 12th IEEE international conference on automatic face & gesture recognition (FG 2017)*, pages 612–618. IEEE, 2017. 8
- [6] James W Cannon, William J Floyd, Richard Kenyon, Walter R Parry, et al. Hyperbolic geometry. *Flavors of geometry*, 31(59-115):2, 1997. 3
- [7] Bike Chen, Wei Peng, Xiaofeng Cao, and Juha Röning. Hyperbolic uncertainty aware semantic segmentation. *IEEE Transactions on Intelligent Transportation Systems*, 2023. 3
- [8] Xinlei Chen and Kaiming He. Exploring simple siamese representation learning. In *Proceedings of the IEEE/CVF conference on computer vision and pattern recognition*, pages 15750–15758, 2021. 6
- [9] Ivana Chingovska, André Anjos, and Sébastien Marcel. On the effectiveness of local binary patterns in face anti-spoofing. In *2012 BIOSIG-proceedings of the international conference of biometrics special interest group (BIOSIG)*, pages 1–7. IEEE, 2012. 8
- [10] Sumit Chopra, Raia Hadsell, and Yann LeCun. Learning a similarity metric discriminatively, with application to face verification. In *2005 IEEE computer society conference on computer vision and pattern recognition (CVPR'05)*, pages 539–546. IEEE, 2005. 5
- [11] Jia Deng, Wei Dong, Richard Socher, Li-Jia Li, Kai Li, and Li Fei-Fei. Imagenet: A large-scale hierarchical image database. In *2009 IEEE conference on computer vision and pattern recognition*, pages 248–255. Ieee, 2009. 6
- [12] HS Eggleston, Leandro Buendia, Kyoko Miwa, Todd Ngara, and Kiyoto Tanabe. 2006 ipcc guidelines for national greenhouse gas inventories. 2006. 2
- [13] Aleksandr Ermolov, Leyla Mirvakhabova, Valentin Khrulkov, Nicu Sebe, and Ivan Oseledets. Hyperbolic vision transformers: Combining improvements in metric learning. In *Proceedings of the IEEE/CVF Conference on Computer Vision and Pattern Recognition*, pages 7409–7419, 2022. 3, 7
- [14] Hervé Fournier, Anas Ismail, and Antoine Vigneron. Computing the gromov hyperbolicity of a discrete metric space. *Information Processing Letters*, 115(6-8):576–579, 2015. 6
- [15] Mark A Friedl, Douglas K McIver, John CF Hodges, Xiaoyang Y Zhang, D Muchoney, Alan H Strahler, Curtis E Woodcock, Sucharita Gopal, Annemarie Schneider, Amanda Cooper, et al. Global land cover mapping from modis: algorithms and early results. *Remote sensing of Environment*, 83(1-2):287–302, 2002. 2
- [16] Songwei Ge, Shlok Mishra, Simon Kornblith, Chun-Liang Li, and David Jacobs. Hyperbolic contrastive learning for visual representations beyond objects. In *Proceedings of the IEEE/CVF conference on computer vision and pattern recognition*, pages 6840–6849, 2023. 3
- [17] Yunhui Guo, Xudong Wang, Yubei Chen, and Stella Yu. Free hyperbolic neural networks with limited radii. 2021. 3, 5
- [18] Yunhui Guo, Xudong Wang, Yubei Chen, and Stella X Yu. Clipped hyperbolic classifiers are super-hyperbolic classifiers. In *Proceedings of the IEEE/CVF Conference on Computer Vision and Pattern Recognition*, pages 11–20, 2022. 5
- [19] Shuangpeng Han, Rizhao Cai, Yawen Cui, Zitong Yu, Yongjian Hu, and Alex Kot. Hyperbolic face anti-spoofing. *arXiv preprint arXiv:2308.09107*, 2023. 3
- [20] Kaiming He, Xiangyu Zhang, Shaoqing Ren, and Jian Sun. Deep residual learning for image recognition. In *Proceedings of the IEEE conference on computer vision and pattern recognition*, pages 770–778, 2016. 6, 8
- [21] Yunpei Jia, Jie Zhang, Shiguang Shan, and Xilin Chen. Single-side domain generalization for face anti-spoofing. In *Proceedings of the IEEE/CVF Conference on Computer Vision and Pattern Recognition*, pages 8484–8493, 2020. 8
- [22] Valentin Khrulkov, Leyla Mirvakhabova, Evgeniya Ustinova, Ivan Oseledets, and Victor Lempitsky. Hyperbolic image embeddings. In *Proceedings of the IEEE/CVF Conference on Computer Vision and Pattern Recognition*, pages 6418–6428, 2020. 2, 3, 5, 6

- [23] Yann LeCun and Fu Jie Huang. Loss functions for discriminative training of energy-based models. In *International workshop on artificial intelligence and statistics*, pages 206–213. PMLR, 2005. 5
- [24] Calvin Ka Fai Lee, Guangqin Song, Helene C Muller-Landau, Shengbiao Wu, S Joseph Wright, KC Cushman, Raquel Fernandes Araujo, Stephanie Bohlman, Yingyi Zhao, Ziyu Lin, et al. Cost-effective and accurate monitoring of flowering across multiple tropical tree species over two years with a time series of high-resolution drone imagery and deep learning. *ISPRS Journal of Photogrammetry and Remote Sensing*, 2019:92–103, 2023. 3, 7, 8
- [25] Ilya Loshchilov and Frank Hutter. Decoupled weight decay regularization. *arXiv preprint arXiv:1711.05101*, 2017. 6
- [26] Maximillian Nickel and Douwe Kiela. Poincaré embeddings for learning hierarchical representations. *Advances in neural information processing systems*, 30, 2017. 3, 5
- [27] Maximillian Nickel and Douwe Kiela. Learning continuous hierarchies in the lorentz model of hyperbolic geometry. In *International conference on machine learning*, pages 3779–3788. PMLR, 2018. 3
- [28] John Y Park, Helene C Muller-Landau, Jeremy W Lichstein, Sami W Rifai, Jonathan P Dandois, and Stephanie A Bohlman. Quantifying leaf phenology of individual trees and species in a tropical forest using unmanned aerial vehicle (uav) images. *Remote Sensing*, 11(13):1534, 2019. 3
- [29] Wei Peng, Jingang Shi, Zhaoqiang Xia, and Guoying Zhao. Mix dimension in poincaré geometry for 3d skeleton-based action recognition. In *Proceedings of the 28th ACM International Conference on Multimedia*, pages 1432–1440, 2020. 3
- [30] Jeffrey J Richardson and L Monika Moskal. Strengths and limitations of assessing forest density and spatial configuration with aerial lidar. *Remote Sensing of Environment*, 115(10):2640–2651, 2011. 3
- [31] Frederic Sala, Chris De Sa, Albert Gu, and Christopher Ré. Representation tradeoffs for hyperbolic embeddings. In *International conference on machine learning*, pages 4460–4469. PMLR, 2018. 1, 3
- [32] Rik Sarkar. Low distortion delaunay embedding of trees in hyperbolic plane. In *International symposium on graph drawing*, pages 355–366. Springer, 2011. 1, 3
- [33] Ramprasaath R Selvaraju, Michael Cogswell, Abhishek Das, Ramakrishna Vedantam, Devi Parikh, and Dhruv Batra. Grad-cam: Visual explanations from deep networks via gradient-based localization. In *Proceedings of the IEEE international conference on computer vision*, pages 618–626, 2017. 8
- [34] Mozhdah Shahbazi, Jérôme Théau, and Patrick Ménard. Recent applications of unmanned aerial imagery in natural resource management. *GIScience & Remote Sensing*, 51(4): 339–365, 2014. 2
- [35] Guofan Shao. Satellite data. *Encyclopedia of environmetrics*, 2006. 2
- [36] Karen Simonyan and Andrew Zisserman. Very deep convolutional networks for large-scale image recognition. *arXiv preprint arXiv:1409.1556*, 2014. 6, 8
- [37] Debjyoti Sinha and Mohamed El-Sharkawy. Thin mobilenet: An enhanced mobilenet architecture. In *2019 IEEE 10th annual ubiquitous computing, electronics & mobile communication conference (UEMCON)*, pages 0280–0285. IEEE, 2019. 7, 8
- [38] Yiyu Sun, Yaojie Liu, Xiaoming Liu, Yixuan Li, and Wen-Sheng Chu. Rethinking domain generalization for face anti-spoofing: Separability and alignment. In *Proceedings of the IEEE/CVF conference on computer vision and pattern recognition*, pages 24563–24574, 2023. 8
- [39] Christian Szegedy, Wei Liu, Yangqing Jia, Pierre Sermanet, Scott Reed, Dragomir Anguelov, Dumitru Erhan, Vincent Vanhoucke, and Andrew Rabinovich. Going deeper with convolutions. In *Proceedings of the IEEE conference on computer vision and pattern recognition*, pages 1–9, 2015. 7, 8
- [40] Lina Tang and Guofan Shao. Drone remote sensing for forestry research and practices. *Journal of Forestry Research*, 26:791–797, 2015. 2
- [41] Xu Tang, Haotian You, Yao Liu, Qixu You, and Jianjun Chen. Monitoring of monthly height growth of individual trees in a subtropical mixed plantation using uav data. *Remote Sensing*, 15(2):326, 2023. 2
- [42] A Trpin and BM Boshkoska. Face recognition with a hyperbolic metric classification model. In *2022 45th Jubilee International Convention on Information, Communication and Electronic Technology (MIPRO)*, pages 317–320. IEEE, 2022. 3
- [43] Laurens Van der Maaten and Geoffrey Hinton. Visualizing data using t-sne. *Journal of machine learning research*, 9(11), 2008. 7, 8
- [44] Chien-Yi Wang, Yu-Ding Lu, Shang-Ta Yang, and Shang-Hong Lai. Patchnet: A simple face anti-spoofing framework via fine-grained patch recognition. In *Proceedings of the IEEE/CVF Conference on Computer Vision and Pattern Recognition*, pages 20281–20290, 2022. 8
- [45] Zhuo Wang, Zezheng Wang, Zitong Yu, Weihong Deng, Jiahong Li, Tingting Gao, and Zhongyuan Wang. Domain generalization via shuffled style assembly for face anti-spoofing. In *Proceedings of the IEEE/CVF conference on computer vision and pattern recognition*, pages 4123–4133, 2022. 8
- [46] Di Wen, Hu Han, and Anil K Jain. Face spoof detection with image distortion analysis. *IEEE Transactions on Information Forensics and Security*, 10(4):746–761, 2015. 8
- [47] George M Woodwell, RoH Whittaker, WA Reiners, Gene E Likens, CC Delwiche, and DB Botkin. The biota and the world carbon budget: The terrestrial biomass appears to be a net source of carbon dioxide for the atmosphere. *Science*, 199(4325):141–146, 1978. 2
- [48] Wen Xiao, Sudan Xu, Sander Oude Elberink, and George Vosselman. Individual tree crown modeling and change detection from airborne lidar data. *IEEE Journal of selected topics in applied earth observations and remote sensing*, 9(8):3467–3477, 2016. 2
- [49] Zhiwei Zhang, Junjie Yan, Sifei Liu, Zhen Lei, Dong Yi, and Stan Z Li. A face antispoofing database with diverse attacks. In *2012 5th IAPR international conference on Biometrics (ICB)*, pages 26–31. IEEE, 2012. 8